A nonlinear inversion for the velocity background and perturbation models

Zedong Wu and Tariq Alkhalifah ,King Abdullah University of Science and Technology

SUMMARY

Reflected waveform inversion (RWI) provides a method to reduce the nonlinearity of the standard full waveform inversion (FWI) by inverting for the single scattered wavefield obtained using an image. However, current RWI methods usually neglect diving waves, which is an important source of information for extracting the long wavelength components of the velocity model. Thus, we propose a new optimization problem through breaking the velocity model into the background and the perturbation in the wave equation directly. In this case, the perturbed model is no longer the single scattering model, but includes all scattering. We optimize both components simultaneously, and thus, the objective function is nonlinear with respect to both the background and perturbation. The new introduced w can absorb the non-smooth update of background naturally. Application to the Marmousi model with frequencies that start at 5 Hz shows that this method can converge to the accurate velocity starting from a linearly increasing initial velocity. Application to the SEG2014 demonstrates the versatility of the approach.

INTRODUCTION

Conventional FWI is based on minimizing the misfit between the predicted and observed wavefields at the sensor locations (Virieux and Operto, 2009). However this objective function is far from smooth or convex, especially with respect the high wavenumber components of the velocity model, which, in the absence of very low frequency, requires a good starting model that is close to the true model to avoid converging to local minimal.

Xu et al. (2012) and Zhou et al. (2012) developed a method based partially on the work of (Plessix et al., 1995) of inverting using reflected energy in the course of FWI, namely RWI. The idea is based on using migration to image the reflections in the data. This image serves as the perturbation in the model necessary to create the reflections. As a result, RWI inverts mainly for the background model, like in MVA, without the need for extended images or angle gathers. Wang et al. (2013) implemented the same approach in the frequency domain to utilize a sequential frequency implementation, which they thought was necessary to avoid some of the nonlinearity brought about by the adjoint nature of the denigration process. Wu and Alkhalifah (2014b) implemented RWI with the spectral method as a wavefield extrapolator (Wu and Alkhalifah, 2014a). They found a new term that has the the opposite direction of the standard two term of RWI and linearly combine them to update the velocity as smooth as possible while guaranteeing the ascending direction of the approximate gradient. Nevertheless, since this method is based on the reflected wave, the direct arrival is usually treated as noise (Tang et al., 2013; Alkhalifah and Choi, 2012). In order to update the background velocity along the wave-path of both diving and reflected waves, Wu and Alkhalifah (2015) propose a new optimization problem based on the Born approximation of reflector, which yields a near linear inversion for the image. They also utilize a scattering angle filter to clean up the gradient and admit only smooth update in the early iterations.

In this abstract, we devise an optimization problem that are nonlinear with respect to both the background and perturbed velocity models, as the perturbed model is not limited to the Born approximation. We, also, apply a scattering angle filter to direct the smooth components of the gradient to the background and non-smooth components to the perturbation model.

THEORY

Standard FWI can be formulated as the following optimization problem

$$\min_m \sum_i \frac{1}{2}\int_t |p(\vec{x}_i,t)-g(\vec{x}_i,t)|^2, \;\; s.t. \;\; p_{tt}-m\Delta p = f, \quad (1)$$

where $\vec{x}_i$ are positions of receivers, g is the relative observed data, p is the wavefield, Δ is the Laplacian operator, and f is the source wavelet. In this abstract, we use $m = v^2$, the square of velocity v, as our model parameter. We split the actual model m_{all} into mainly background (m) and perturbed (w) components, which means $m_{all} = m + w$. We also define the corresponding wavefield as $p_{all} = p + q$, where p is the wavefield corresponding to modeling from the source using m, and q is the wavefield difference mainly resulting from the perturbation, w, and using the velocity m. Thus, p_{all} satisfies the wave equation for $m+w$, given by

$$(p+q)_{tt} - (m+w)\Delta(p+q) = f. \quad (2)$$

In addition, the background wavefield satisfies

$$p_{tt} - m\Delta p = f. \quad (3)$$

Subtracting (3) from (2), we obtain the equation for the perturbed wavefield as

$$q_{tt} - m\Delta q - w\Delta q = w\Delta p. \quad (4)$$

Up to this point, no approximation were used, and thus, equation (4) is exact within the rim of assumption considered here (acoustic). In the spirit of Alkhalifah and Wu (2015), instead of solving the optimization problem (1), we solve the following optimization problem

$$\min_{m,w} J(p,q) = \frac{1}{2}\sum_i \int_t |p(\vec{x}_i,t)+q(\vec{x}_i,t)-g(\vec{x}_i,t)|^2, \quad (5)$$

$$s.t. \;\; p_{tt} - m\Delta p = f, \; q_{tt} - m\Delta q - w\Delta q = w\Delta p. \quad (6)$$

Here, w is independent of m. Instead of optimizing only m, which is done in standard FWI and RWI, we optimize both m and w, simultaneously. Let us denote the standard and perturbed wave equation as

$$Lp = p_{tt} - m\Delta p \quad (7)$$

$$\tilde{L}q = q_{tt} - m\Delta q - w\Delta q. \quad (8)$$

DOI http://dx.doi.org/10.1190/segam2015-5846177.1

The gradient of optimization (5) can be easily derived as

$$\nabla_m J = \int_t \lambda \Delta p + \tilde{\lambda} \Delta q + \mu \Delta p \quad (9)$$

$$\nabla_w J = \int_t (\Delta p + \Delta q) \tilde{\lambda}, \quad (10)$$

where

$$\lambda = L^{-T}(p(\vec{x}_i,t) + q(\vec{x}_i,t) - g(\vec{x}_i,t)), \quad (11)$$

$$\tilde{\lambda} = \tilde{L}^{-T}(p(\vec{x}_i,t) + q(\vec{x}_i,t) - g(\vec{x}_i,t)), \quad (12)$$

$$\mu = L^{-T}(\Delta(\tilde{\lambda} w)) \quad (13)$$

Scattering angle control

When $w = 0$, the gradient with respect to m will be the standard FWI gradient. We use a filter (Alkhalifah, 2015) to update m smoothly while placing the non smooth components into w. To do so efficiently, we utilize an approximate and cheap scattering angle filter proposed in Wu and Alkhalifah (2015). It is based on the time-shift imaging condition(Sava and Fomel, 2006; Khalil et al., 2013). Let us denote $I(x)$ as one of the components of the above gradient (9), which is is the cross correlation of two wavefield u_s and u_r. That's $I(x) = \int_t u_s(x,t) u_r(x,t) dt$. Here u_s and u_r are arbitrary forward and backward propagating wavefields in equation (9). An approximate scattering angle filter formulation can be defined as

$$I^n_f(x) = v^n \int_{k_x} \int_{\omega_t} \frac{|k_x|^n}{\omega_t^n} \hat{I}(k_x, \omega_t) e^{i k_x \cdot x}. \quad (14)$$

In which, n is a parameter of filtering. When $n < 0$, it will enhance the large scattering angle, which is used to update m. When $n > 0$, it will enhance the small scattering angle and we apply it to update of w. In both examples below, we set $n = 2$ for the gradient of w and n negative to update m.

EXAMPLES

Our first example is the Marmousi model. Figure 1a shows the exact Marmousi velocity model. We add a thin water layer on the surface to reduce the source illumination and increase the difficulty of the problem. The wavefields are extrapolated on a mesh size of 32 m by 32 m. Using a band pass filtered Ricker wavelet to remove frequencies below 5 Hz and most of the high frequencies, we generate data that we refer to as observed. We include in the model the free surface multiple for both modeling and inversion. The shot interval is 256 m and every grid points on the surface acts as a receiver. During the inversion procedure, we don't update v, w in the water layer and we set v to the exact water velocity and $w = 0$. The initial velocity is linearly increasing with depth from 1500 m/s to 4000 m/s, as shown in Figure 1b and the initial $w = 0$. We apply the above described inversion with $n = -3.0,\ -2.0,\ -1.5,\ -1.0,\ -0.5,\ 0$ for updating m sequentially. The inverted velocity is shown in Figure 1c. For comparison, we apply the standard FWI procedure to the same dataset, the inverted velocity is shown in Figure 1d. We can see easily that the standard FWI stopped at some local minimum. Figure 2a shows the exact seismogram at the center shot. Figure 2b, 2c, 2d show the difference between the exact seismogram and the one modeled by the initial, our inverted velocity and the inverted velocity using standard FWI plotted at the same scale. We can see that residual obtained using our method is much smaller than that obtained using the inverted one by standard FWI.

Our next example is the SEG2014 dataset that was modeled externally, and thus, the extrapolation tools used here are different than those used in generating the observed data. It was actually distributed as a blind test for Full waveform inversion (FWI). The dataset includes 1600 shots records with 25 m shot sampling at a depth of 15 m. Each shot has 321 receivers with 25 m sampling at the depth of 15 m. Though the data represent a marine acquisition, they were acquired using elastic modeling in which some of the events may correspond to converted waves. The data are generated with an isotropic elastic wave equation with free surface multiple, and has low signal-to-noise ratio below 3 Hz. The maximum recording time is 8 s. To reduce the computational cost associated with the inversion, we invert for one in every eight shots. An initial velocity was provided and shown in Figure 3a. We apply the inversion with 30 m depth and 50 m lateral interval spacing and 4 ms time sampling at the early stage. Later (higher frequencies), we reduce the space sampling to 30 m by 25 m. First we apply a bandpass filter to the data with truncated frequency of 3.5 Hz. We apply the proposed inversion, followed by conventional FWI with the data spectrum extending to frequencies of 4.0 Hz, 4.5 Hz, and 5.0 Hz. We stopped at 5 Hz due to time constraints, and we plan to show further results at the presentation. The inverted velocity is shown in Figure 3b. Even though we did not go to very high frequency and the data is modeled using the elastic wave equation, we can still see some interesting features such as the three abnormal low velocity zones. We can also see some velocity discontinuities. To confirm the improvement of the velocity, we compare the received data (Figure 3c), the data modeled by the initial (Figure 3d) and inverted (Figure 3e) velocity. Figure 4a and 4b show the comparison of RTM extracted by the initial and inverted velocity. For quantitative comparison, we show the angle gather extracted by the initial (Figure 4c) and inverted velocity (Figure 4d). At last, the dataset provides a wellog at $x = 39375\ m$, we show it in Figure 4e. All the quantitative comparisons show that the proposed FWI method can improve the velocity.

CONCLUSIONS

We formulated a new optimization problem to invert for the background model and the perturbation, simultaneously. The objective function minimizes the residuals between the observed data and those data modeled from the source and the perturbations . By applying a scattering angle filter, we can update the background model with smooth components and perturbation model with the scattering components.

ACKNOWLEDGEMENTS

We thank KAUST for its support and the SWAG group for collaborative environment. We thank CHEVRON for providing the SEG2014 benchmark dataset.

DOI http://dx.doi.org/10.1190/segam2015-5846177.1

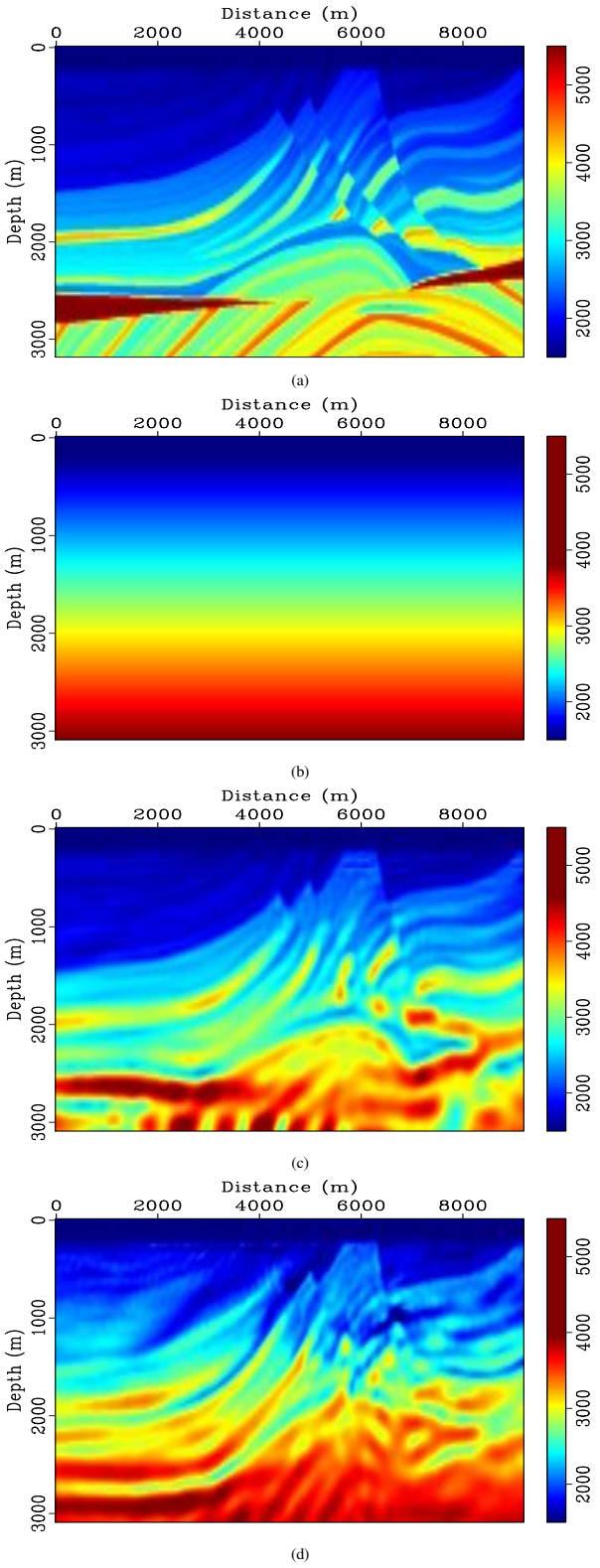

Figure 1: (a) The exact Marmousi model. (b) The initial velocity. (c) The inverted velocity with the proposed method. (d) The inverted velocity with standard FWI.

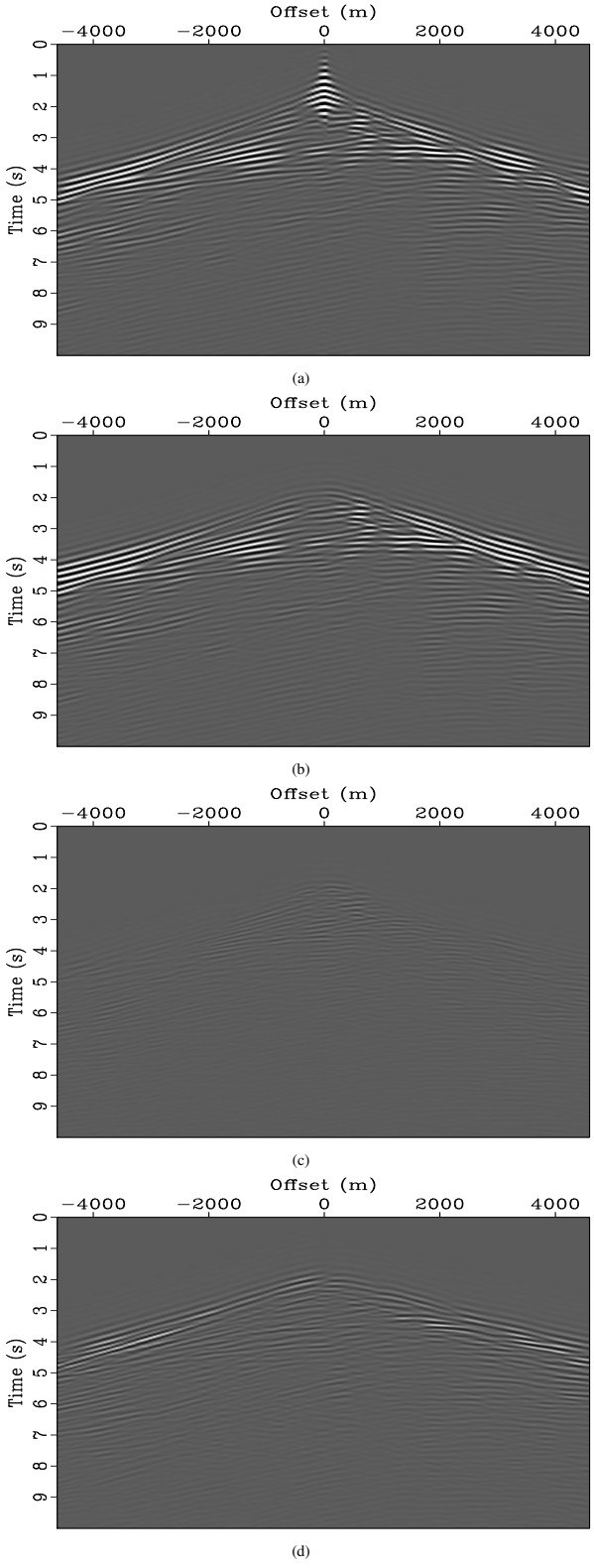

Figure 2: (a) The actual seismogram. (b) Residual seismogram with those corresponding to the initial velocity. (c) Residual seismogram with those corresponding to the inverted velocity. (d) Residual seismogram with those corresponding to the inverted velocity from standard FWI.

DOI http://dx.doi.org/10.1190/segam2015-5846177.1

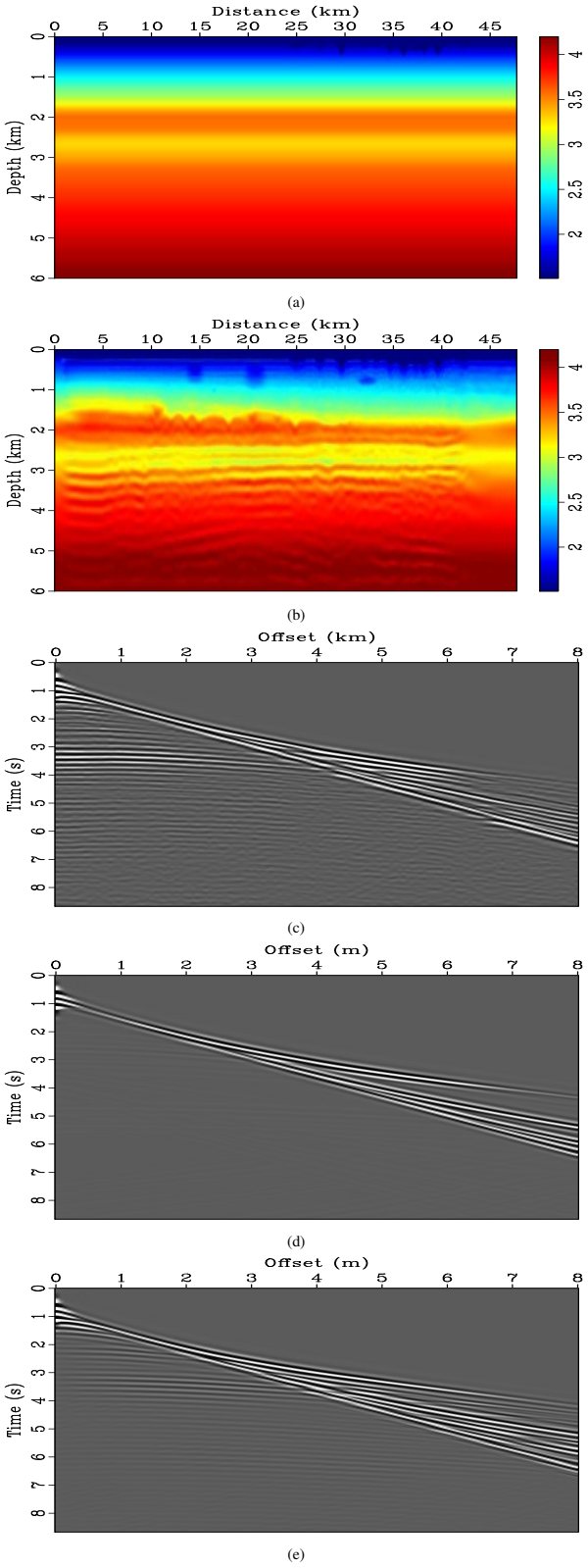

Figure 3: (a) The initial velocity. (b) The inverted velocity. (c) The observed data. (d) Modeled data using the initial velocity. (e) Modeled data using the inverted velocity.

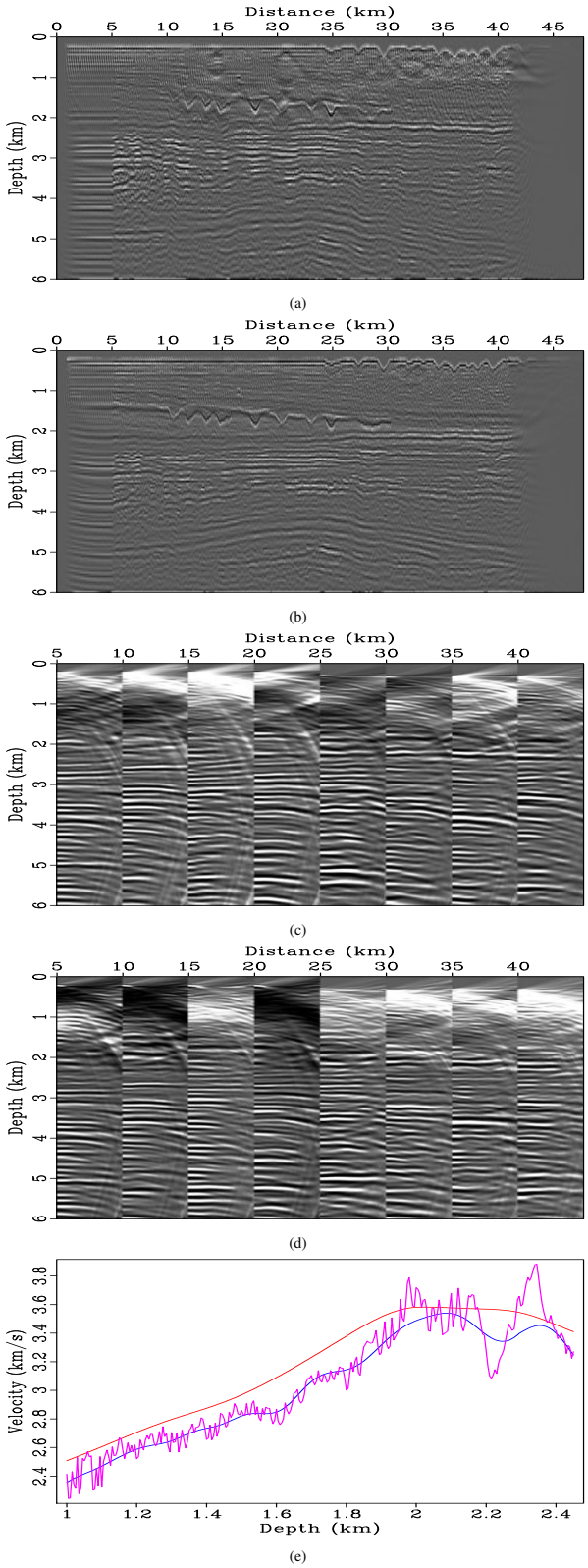

Figure 4: An RTM image resulting from the initial (a), and the inverted velocity (b). Angle gathers corresponding to imaging with the initial velocity (c) and with inverted velocity (d) from 0^o to 45^o. (e) The well-log comparison.

DOI http://dx.doi.org/10.1190/segam2015-5846177.1

EDITED REFERENCES

Note: This reference list is a copyedited version of the reference list submitted by the author. Reference lists for the 2015 SEG Technical Program Expanded Abstracts have been copyedited so that references provided with the online metadata for each paper will achieve a high degree of linking to cited sources that appear on the Web.

REFERENCES

Alkhalifah, T., 2015, Scattering-angle based filtering of the waveform inversion gradients: Geophysical Journal International, **200**, no. 1, 363–373, http://dx.doi.org/10.1093/gji/ggu379.

Alkhalifah, T., and Y. Choi, 2012, Taming waveform inversion non-linearity through phase unwrapping of the model and objective functions: Geophysical Journal International, **191**, no. 2, 1171–1178.

Alkhalifah, T., and Z. Wu, 2014, FWI and MVA the natural way: 76th Conference & Exhibition, EAGE, Extended Abstracts, doi:10.3997/2214-4609.20141091.

Khalil, A., J. Sun, Y. Zhang, and G. Poole, 2013, RTM noise attenuation and image enhancement using time-shift gathers: 83rd Annual International Meeting, SEG, Expanded Abstracts, 494–498, http://dx.doi.org/10.1190/segam2013-0600.1.

Plessix, R.-E., Y.-H. De Roeck, and G. Chavent, 1995, Automatic and simultaneous migration velocity analysis and waveform inversion of real data using a MBTT/WKB J formulation: 75th Annual International Meeting, SEG, Expanded Abstracts, 1099–1102.

Sava, P., and S. Fomel, 2006, Time-shift imaging condition in seismic migration: Geophysics, **71**, no. 6, S209–S217, http://dx.doi.org/10.1190/1.2338824.

Tang, Y., S. Lee, A. Baumstein, and D. Hinkley, 2013, Tomographically enhanced full wavefield inversion: 83rd Annual International Meeting, SEG, Expanded Abstracts, 1037–1041, http://dx.doi.org/10.1190/segam2013-1145.1.

Virieux, J., and S. Operto, 2009, An overview of full-waveform inversion in exploration geophysics: Geophysics, **74**, no. 6, WCC1–WCC26, http://dx.doi.org/10.1190/1.3238367.

Wang, S., F. Chen, H. Zhang, and Y. Shen, 2013, Reflection-based full waveform inversion (RFWI) in the frequency domain: 83rd Annual International Meeting, SEG, Expanded Abstracts, 877–881.

Wu, Z., and T. Alkhalifah, 2014a, The optimized expansion based low-rank method for wavefield extrapolation: Geophysics, **79**, no. 2, T51–T60, http://dx.doi.org/10.1190/geo2013-0174.1.

Wu, Z., and T. Alkhalifah, 2014b, Spectral implementation of full waveform inversion based on reflections: 76th Conference & Exhibition, EAGE, Extended Abstracts, doi:10.3997/2214-4609.20140853.

Wu, Z., and T. Alkhalifah, 2015, An improved full waveform inversion procedure based on scattering angle enrichment: 77th Conference & Exhibition, EAGE, Extended Abstracts, Th N104 15, doi:10.3997/2214-4609.201413211.

Xu, S., D. Wang, F. Chen, G. Lambaré, and Y. Zhang, 2012, Inversion on reflected seismic wave: 82nd Annual International Meeting, SEG, Expanded Abstracts, http://dx.doi.org/10.1190/segam2012-1473.1.

Zhou, H., L. Amundsen, and G. Zhang, 2012, Fundamental issues in full waveform inversion: 82nd Annual International Meeting, SEG, Expanded Abstracts, http://dx.doi.org/10.1190/segam2012-0878.1.